A NOVEL TUMOR-IMMUNE MICROENVIRONMENT (TIME)-ON-CHIP MIMICS THREE DIMENSIONAL NEUTROPHIL-TUMOR DYNAMICS AND NEUTROPHIL EXTRACELLULAR TRAPS (NETs)- MEDIATED COLLECTIVE TUMOR INVASION

Vikram Surendran, Dylan Rutledge, Ramair Colmon, and Arvind Chandrasekaran*

Bioinspired Microengineering Laboratory, Department of Chemical, Biological and Bio Engineering, North Carolina A&T State University, Greensboro, USA 27411

*Corresponding author: **Email**: achandra@ncat.edu; **Ph**: (336) 2853721

Supplementary Figures

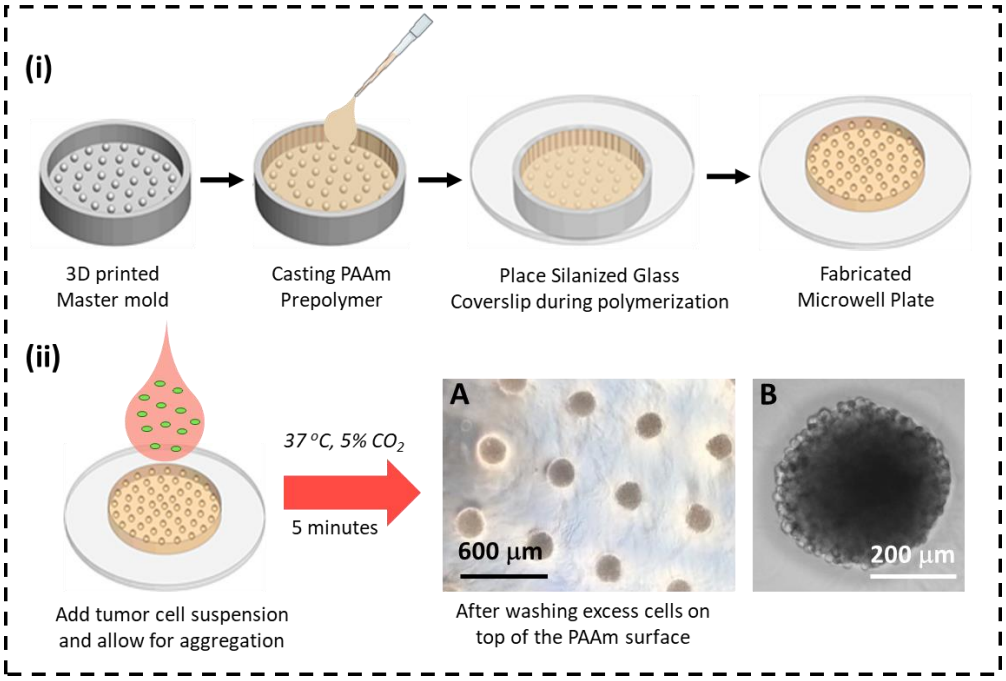

Figure 1S: Schematic fabrication process of the Spheroid multiwell plate- Microwells are created by replica molding process by casting pre-polymerized Polyacrylamide onto 3D printed master molds, attachment with a glass coverslip and removal upon polymerization, retaining the microwell features in the hydrogel (ii) Tumor cell suspension is added on top of the polyacrylamide surface and the device is incubated. Cells enter the microwells and aggregate together, washing away the remaining cells on top of the hydrogel surface leaves tumor cell aggregates with (A) precise positioning and (B) circularity, for further handling and culture manipulations.

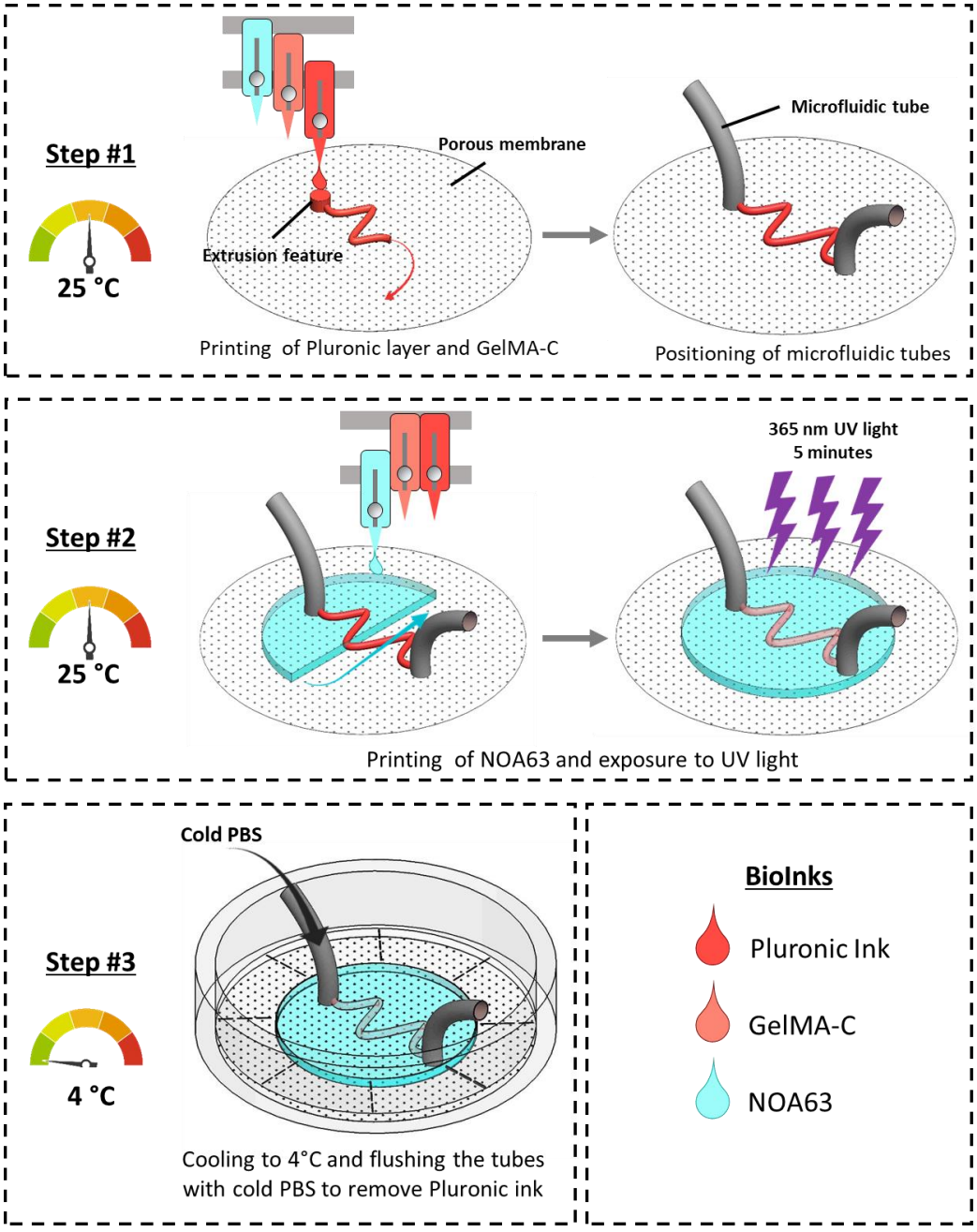

Figure 2S: Schematic semi-automated process for the fabrication of the microchannel using 3D Bioprinter
Step 1: A layer of Pluronic ink of desired microfluidic channel design and height is printed on top of a track-etched membrane at room temperature. A thin layer of GelMA-C ink is printed on top of the pluronic layer for support. Extrusion features are provided for the inlet and outlet tube positioning.
Step 2: UV curable NOA 63 is printed on top covering the channel layer and the setup is exposed to UV light for 5 minutes for curing at room temperature.
Step 3: The porous membrane is attached to a hollow culture dish, and the setup is cooled down on the printer bed to 4 ^{o}C after which cold PBS is flushed through the microfluidic tubes to remove the Pluronic ink and create perfusable microfluidic channels on a porous membrane.

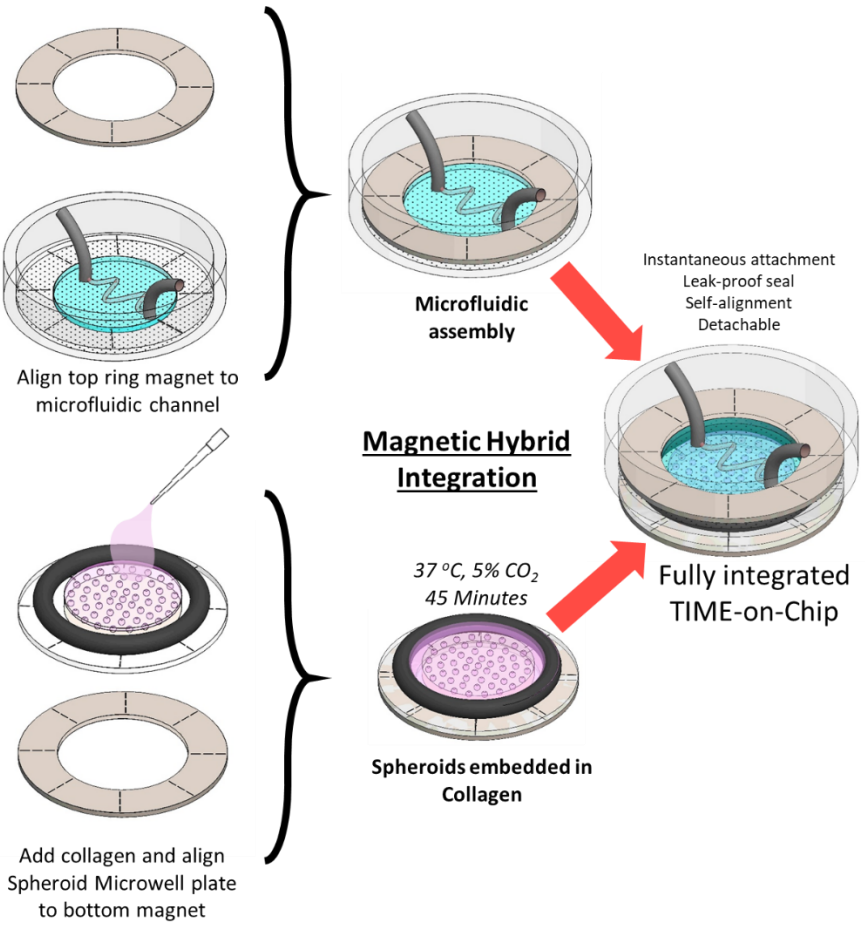

Figure 3S: Schematic Hybrid-integration process: Ring magnet is placed and aligned with the hollow culture dish containing the microfluidic channel. The spheroids microwell plate is placed on another ring magnet and aligned with respect to the pre-made alignment marks. An O-ring is placed on top of the microwell plate and collagen is added inside the O-ring. After the gelation of collagen, both the assemblies are brought in proximity to each other for instantaneous magnetic attachment, and creation of the integrated TIME-on-Chip device.

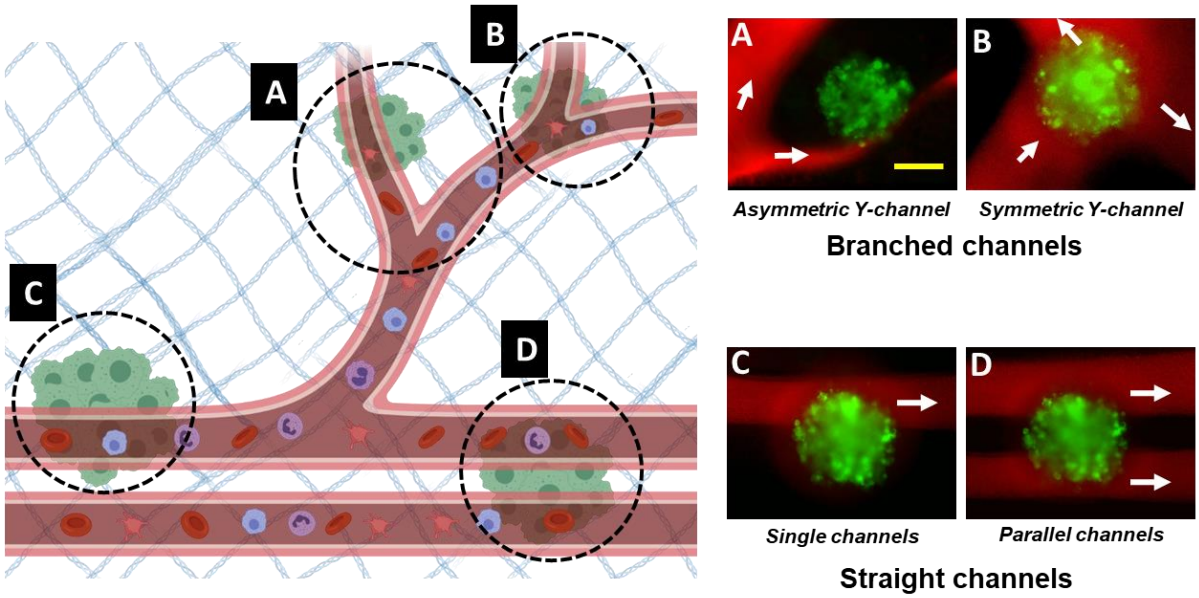

Figure 4S: 3D bioprinting enables the fabrication of different microfluidic channel designs (with fluorescence from Dextran (red)) on the porous membrane, aligned and integrated with the spheroids (green) to mimic different in-vivo-like tumor-vasculature configurations. Arrow indicate the direction of flow (Scale bar represents 200 μm)

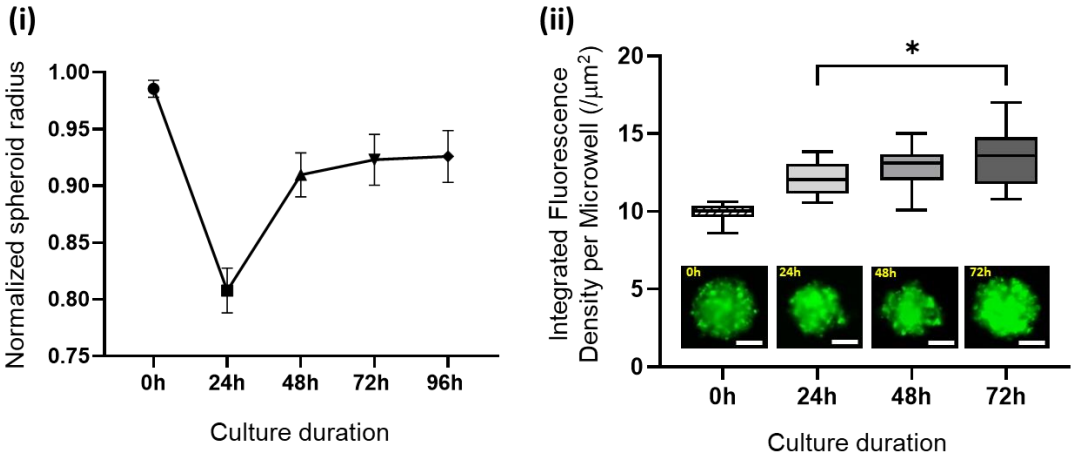

Figure 5S: (i) Initial spheroid formation in the microwell plate consisted of at least three distinct phases, wherein initial aggregation of isolated cells within the microwells was followed by spheroid compaction over 24h and subsequent growth, consistent with previous observations [R1].
(ii) Integrated fluorescence density of OVCAR-3 spheroids expressing GFP increases over 72h

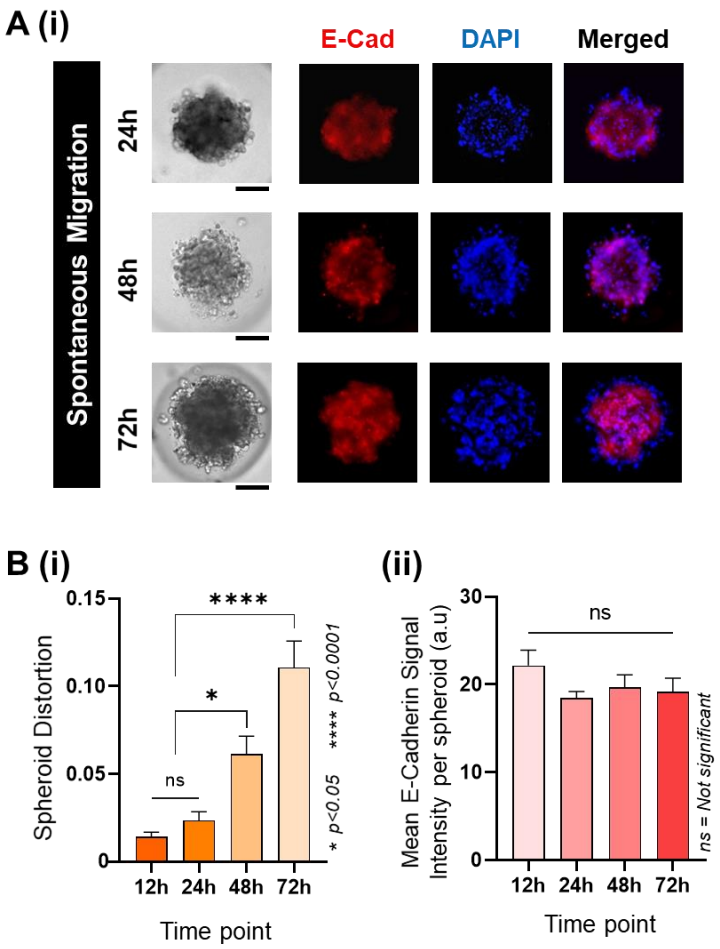

Figure 6S: Spontaneous 3D migration behavior of OVCAR-3: **A**(i) Representative images upon fluorescent immunostaining of OVCAR-3 spheroids at different time points of spontaneous migration for E-cadherin(red) and nuclear stain (DAPI blue) (Scale bars represent 100 μm).

B (i) OVCAR-3 spheroids showed conserved spontaneous migration, and largely remained clustered when present within a 3D collagen matrix, the spheroid distortion was negligible within the first 24h and thereafter marginally increased over the next 48h.

(ii) However, no significant difference was observed in the mean E-cadherinsignal intensity during the spontaneous migration (data collected from n = 9 spheroids, mean ± SEM. Significance was determined using one-way ANOVA with Tukey's post-hoc analysis * p<0.05, ****p<0.0001, ns = not significant)

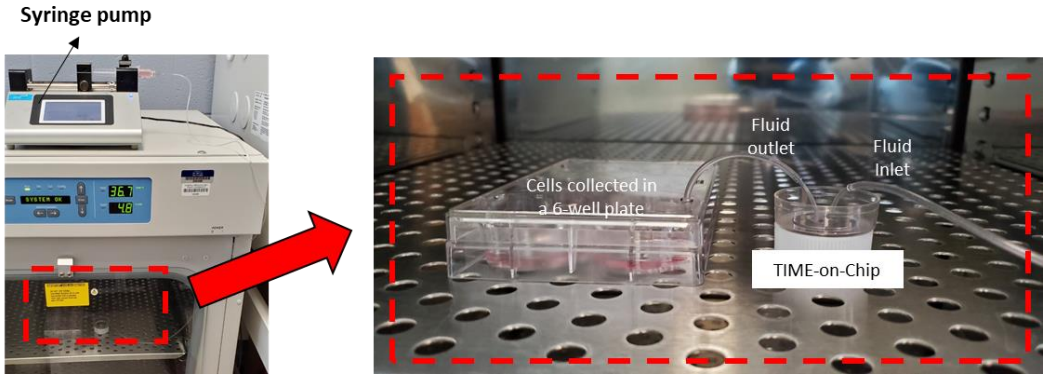

Figure 7S: TIME-on-Chip facilitates fluid flow in the channel when connected with an external syringe pump. The fluid at the outlet could also be collected for further analysis

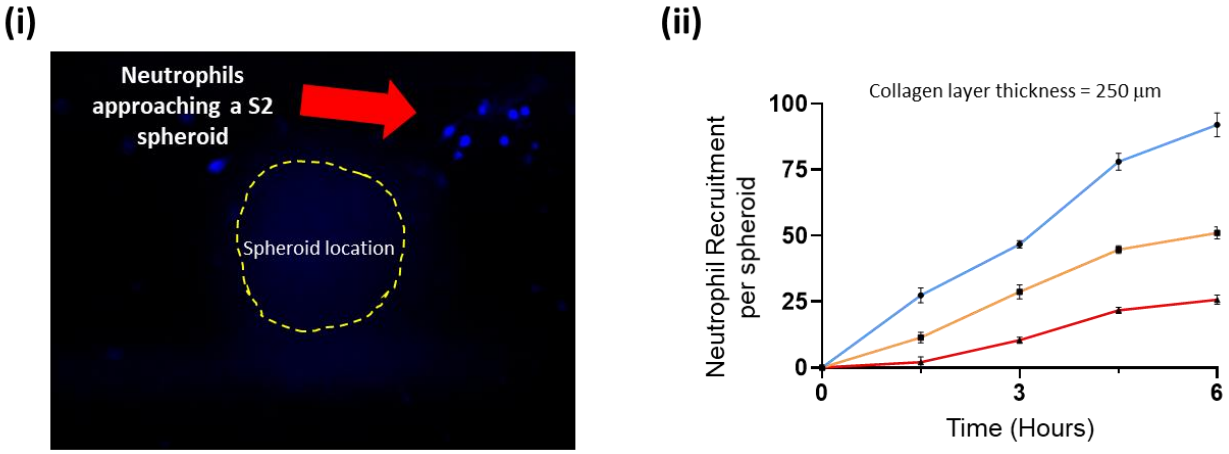

Figure 8S: (i) Neutrophils respond to the spheroids through chemotaxis as early as within 30 minutes and (ii) the infiltration of the neutrophils into the spheroids stabilizes at ~6h

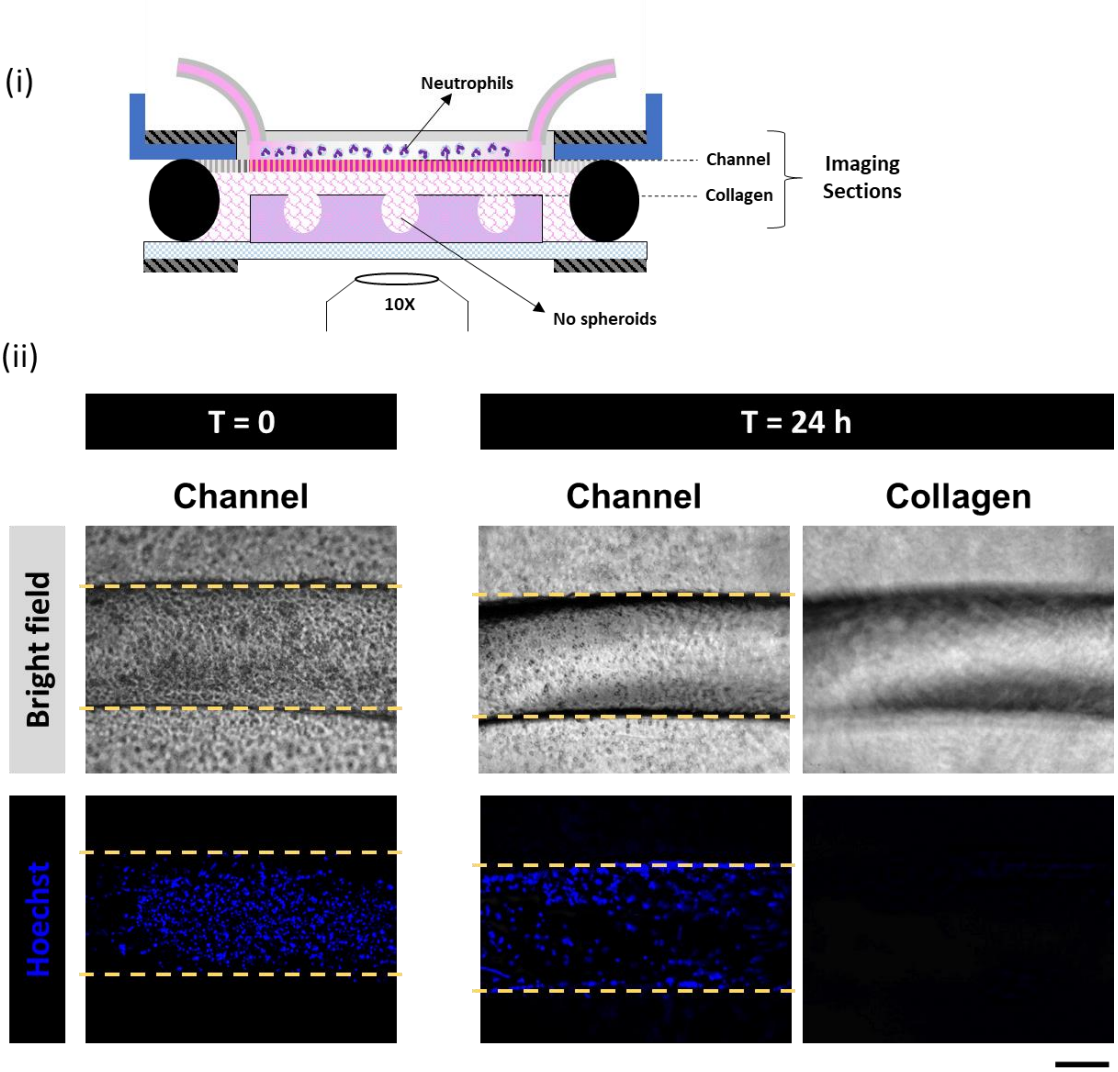

Figure 9S: (i) Random migration of the Hoechst-stained neutrophils from the channel into the collagen region was observed over 24h as schematically shown (ii) No neutrophils were seen in the collagen region, and in the absence of any spheroids all the neutrophils were confined to the microfluidic channel under both flow and no-flow conditions, thereby confirming that neutrophils respond to the tumor spheroids through chemotaxis (Scale bar 100 μm).

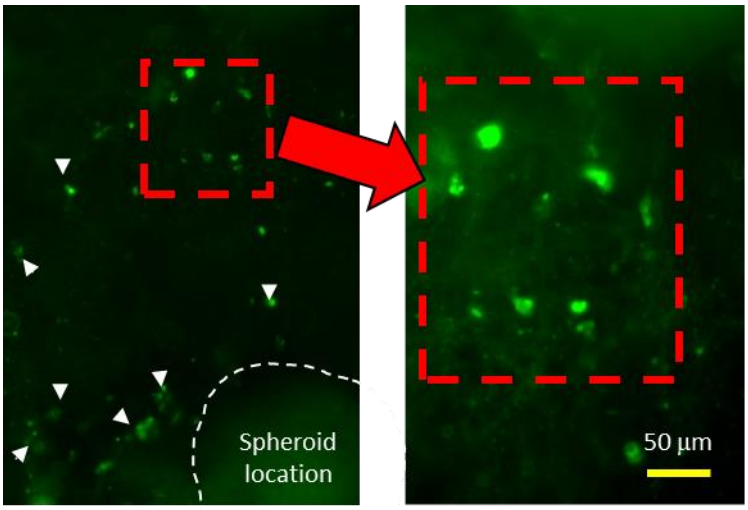

Figure 10S: NETs produced by the infiltrating neutrophils in the stromal collagen region indicated by the arrow marks and within the box) in general had a greater spread area than the NETs produced by the tumor infiltrating neutrophils . At higher magnification, fine fibrils of NETs structures formed in the collagen region were visible.

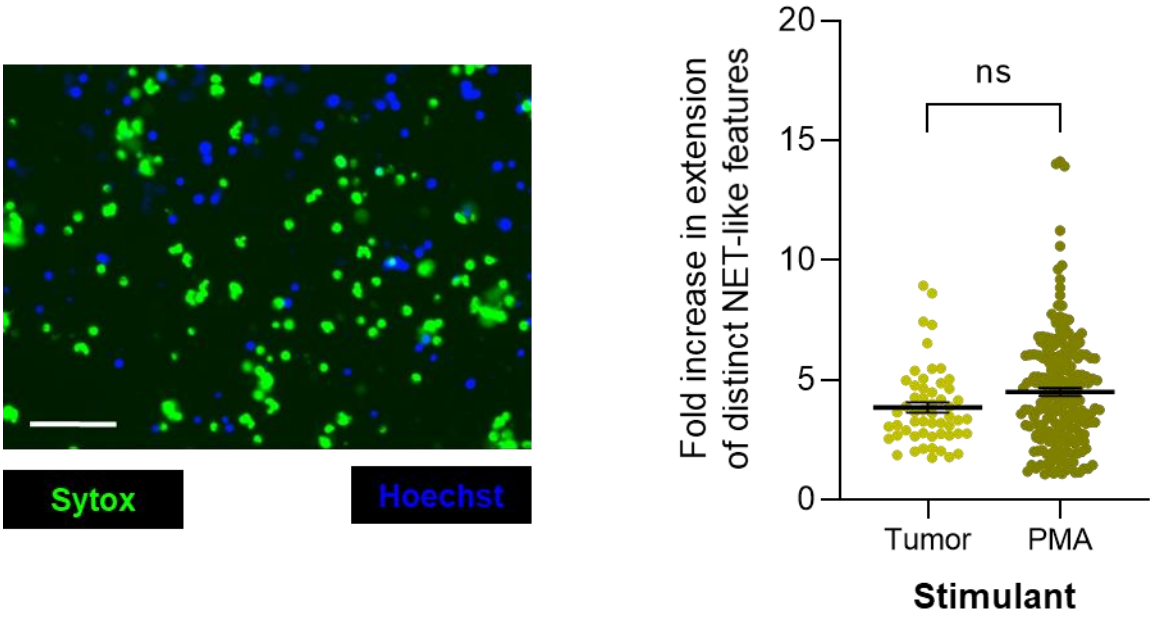

Figure 11S: NET-like structures (Sytox green) produced by the neutrophils embedded within collagen matrix doped with 500 nM PMA (Scale bar 75 µm). No significant difference was observed between the spread areas of the NET-like features observed within PMA doped collagen to those formed by the neutrophils migrating towards the spheroids.

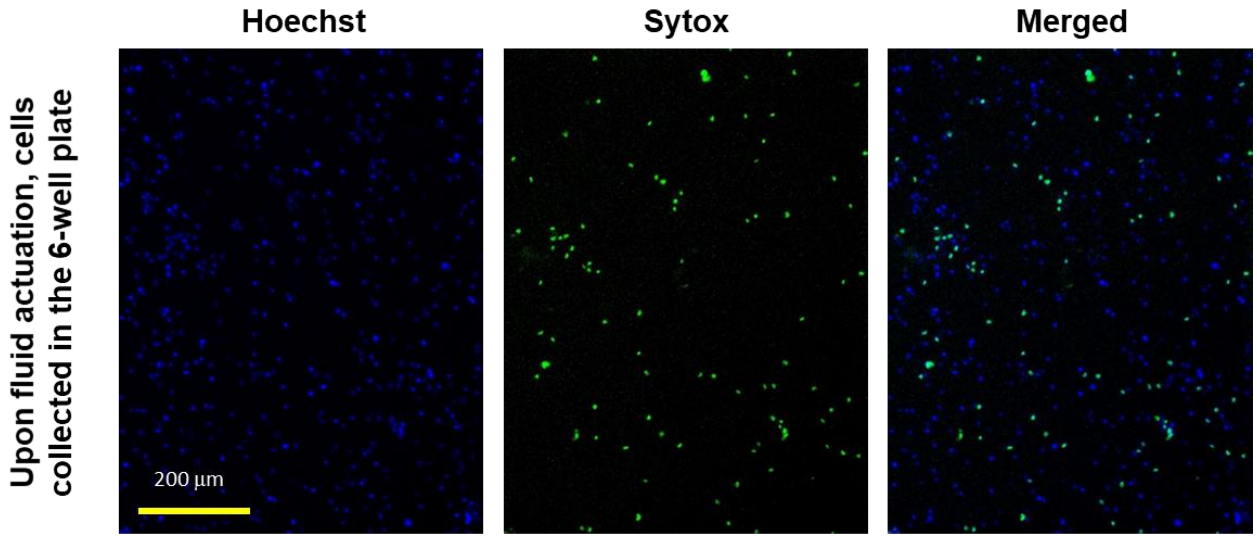

Figure 12S: At the end of 6h neutrophil – tumor interaction assay with flow enabled in the microfluidic channel, cells collected in a 6-well plate from the channel outlet of the TIME-on-Chip shows some of the neutrophils (stained with Hoechst blue) showed condensed NETs features stained by Sytox green

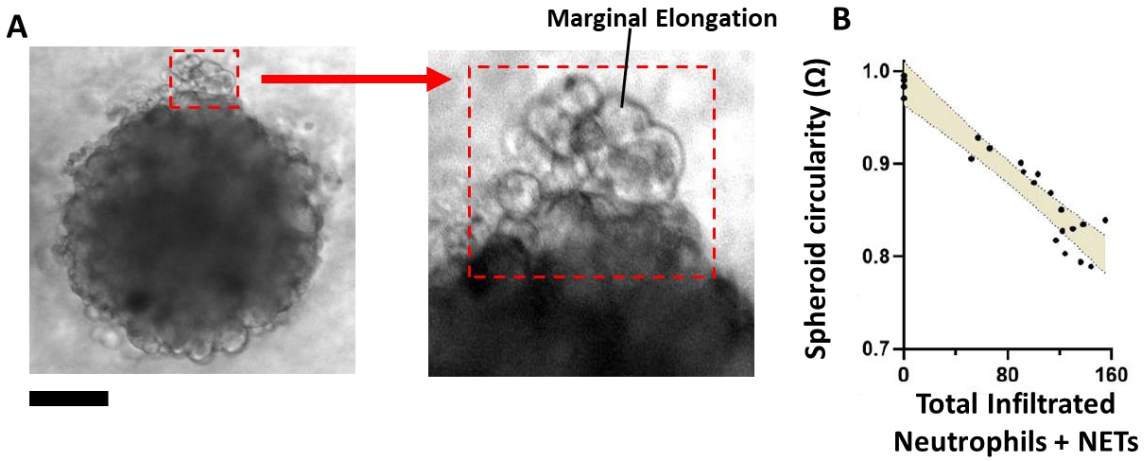

Figure 13S. At the end of 6h neutrophil infiltration assay, the stability of the spheroids denoted by their circularity. **A**. Bright field image of a spheroid with marginal elongation along the periphery (Scale bar represents 125 µm) **B**. Spheroid circularity decreased linearly within 95% confidence interval, with an increase in the cumulative total of the tumor-infiltrated neutrophils and the inter-spheroidal NETs (R^2 = 0.9135).

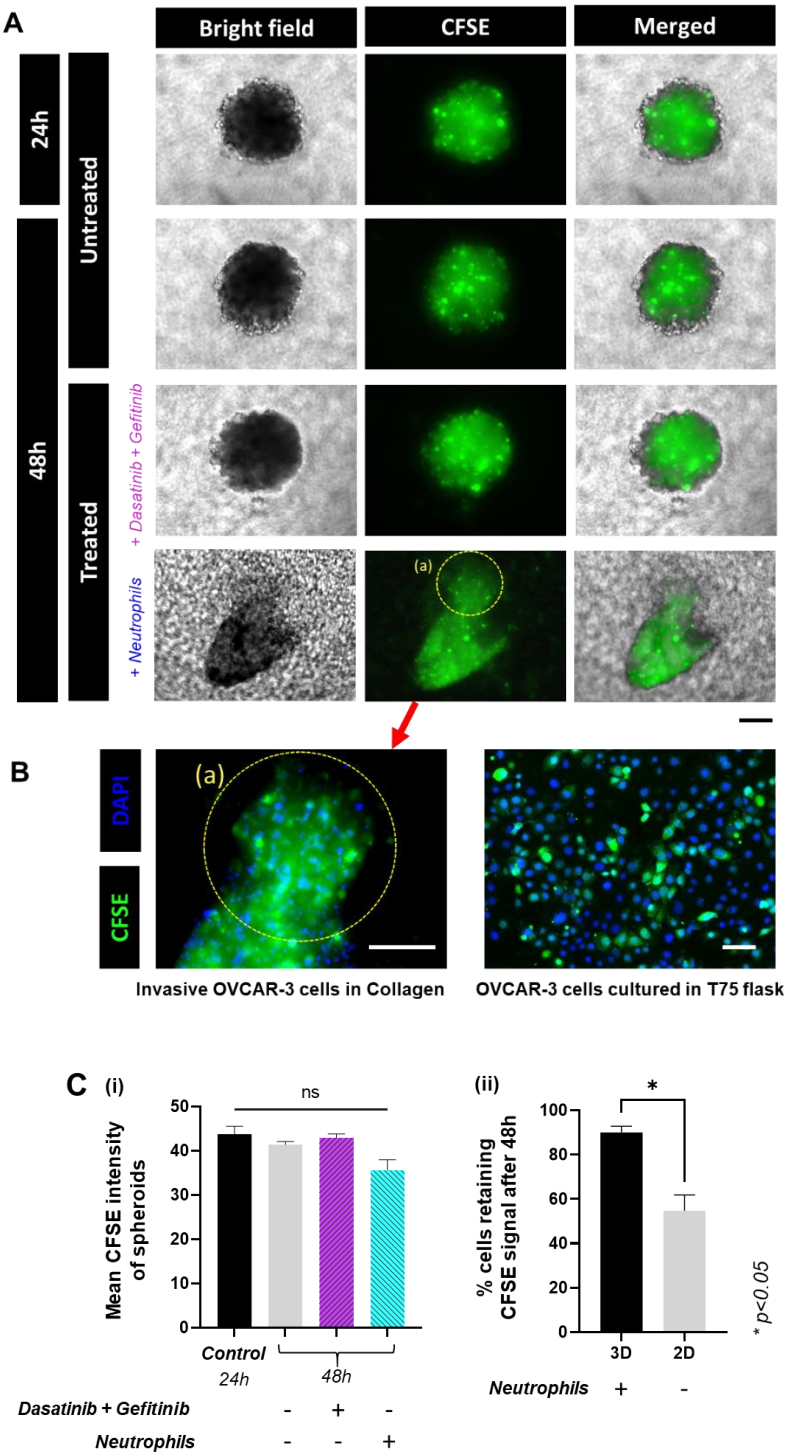

Figure 14S: (A) Images of the spheroids stained with cellTrace CFSE proliferation marker. To evaluate the effect of proliferation of the spheroids in the collagen matrix, cells were treated with a combination of Dasatinib and Gefitinib, and the mean fluorescent signal intensity was compared with the spheroids distored in the presence of NETs (B) Representative fluorescence images of the cells invading into the collagen expressing CFSE compared with the cells simultaneously cultured in a regular 2D cell culture flask.

(C) (i) No significant difference was observed in the mean CFSE signal intensity between the drug treated spheroids, distorted spheroids and untreated spheroids (ii) However, the fraction of cells that retained CFSE

marker in 3D were significantly higher than in 2D culture over 48h suggesting that spheroid distortion observed in the presence of NETs is significantly regulated by invasion than cell proliferation. Scale bars represent 100 μm

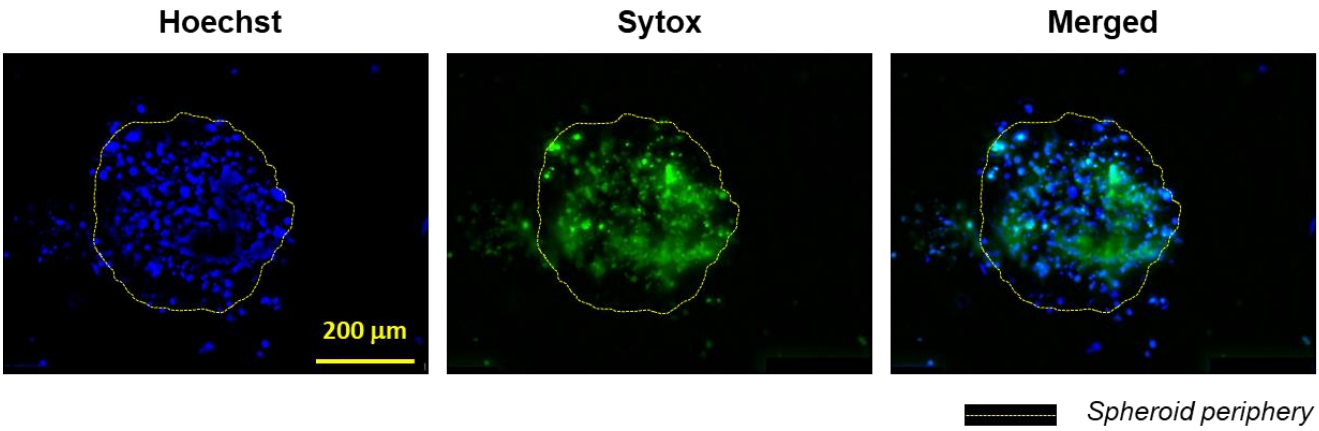

Figure 15S: Neutrophils seeded directly on top of the OVCAR-3 spheroids prior to the addition of collagen gel on top produced substantial NETs. A few of neutrophils migrated to the collagen region surrounding the spheroids, and small NET-like features were observed among them. But the resultant spheroid distortion was negligible.

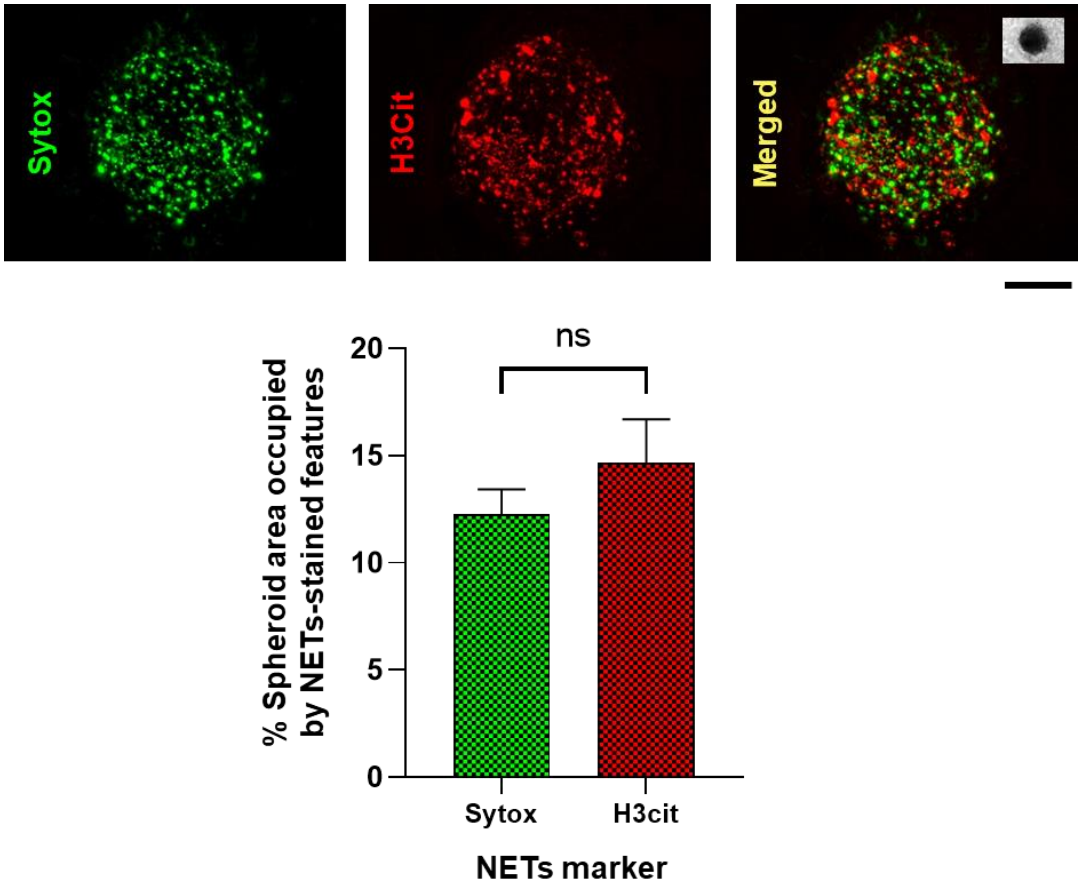

Figure 16S: To verify whether Sytox stained dead tumor cells in the presence of NETs, neutrophils were added directly to the spheroids, and immunostained for Citrullinated histone H3, a NETs-specific marker. Fluorescent images of Sytox (green) and citrullinated H3 (red) were compared. No significant different was observed in the percentage spheroid area occupied by NET-like features observed with both the markers, suggesting that tumor cells remained largely viable in the presence of NETs, and that Sytox signal observed is largely from NETs (Scale bar 100 μm).

Figure 17S: Implementation of an interconnected TIME-on-Chips system on a glass-bottom 12-well plate (upon removing the glass and replacing with the spheroid microwell plate). The magnetically enabled hybrid integration concept could also be readily implemented on a Transwell insert, for user-friendly control of the microenvironments of the cultured cells

Supplementary Information

S1. Calculation of diffusion coefficient for COMSOL modeling

Since Dextran is a large molecule diffusing through a liquid with properties that hinder diffusion of large molecules, a modified version of the Stokes-Einstein equation taking into account fibrous hindrance from the collagen matrix is used for calculating the diffusion coefficient (D_c) given by the expression,

$D_c = kT(R_m)^{-1}$ … (1)

where R_m, the matrix resistance. The expression for R_m is given as $6\pi\mu r_s$ x Hf , with μ being the viscosity of water, and r_s being the radius of the diffusing particle, and Hf is the diffusion hindrance coefficient [R2]. For dextran of molecular weight MW, the particle radius was calculated using the expression [R3]

$R_D = 0.33(MW^{0.46})$ ….. (2)

The diffusion hindrance coefficient of water to collagen is 0.94 [R4], and the dynamic viscosity of water is 8.9×10^{-4} Pa.s. With Boltzmann's constant ($k = 1.38 * 10^{-23}$), and a room temperature of (T = 298.15K), the diffusion coefficient (D_c) was calculated to be 4.12×10^{-11} m^2/s.

Supplementary References

[R1] Smyrek, I., Mathew, B., Fischer, S.C., Lissek, S.M., Becker, S. and Stelzer, E.H.K., 2019. E-cadherin, actin, microtubules and FAK dominate different spheroid formation phases and important elements of tissue integrity. Biology open, 8(1).

[R2] Stylianopoulos, T., Poh, M.Z., Insin, N., Bawendi, M.G., Fukumura, D., Munn, L.L. and Jain, R.K., 2010. Diffusion of particles in the extracellular matrix: the effect of repulsive electrostatic interactions. Biophysical journal, 99(5), pp.1342-1349.

[R3] Aimar, P., Meireles, M. and Sanchez, V., 1990. A contribution to the translation of retention curves into pore size distributions for sieving membranes. Journal of membrane science, 54(3), pp.321-338.

[R4] Truong, D., Puleo, J., Llave, A., Mouneimne, G., Kamm, R.D. and Nikkhah, M., 2016. Breast cancer cell invasion into a three dimensional tumor-stroma microenvironment. Scientific reports, 6, p.34094.